

# H-Band and Spectroscopic Properties of Abell 1644

Aaron W. Tustin, Margaret J. Geller, and Scott J. Kenyon<sup>1</sup>

*Harvard-Smithsonian Center for Astrophysics, 60 Garden Street, Cambridge, MA 02138*

atustin@cfa.harvard.edu, mgeller@cfa.harvard.edu, skenyon@cfa.harvard.edu

and

Antonaldo Diaferio

*Università degli Studi di Torino, Dipartimento di Fisica Generale Amedeo Avogadro,  
Torino, Italy*

diaferio@ph.unito.it

## ABSTRACT

We discuss  $H$ -band ( $1.65 \mu\text{m}$ ) near-infrared photometry of the central  $9 h^{-2}$   $\text{Mpc}^2$  of Abell 1644 to a limiting  $M_H \sim M_H^* + 3$  (throughout this paper  $H_0 = 100h$   $\text{km s}^{-1} \text{Mpc}^{-1}$ ). There are 861 galaxies in the photometric survey region. We also measured radial velocities of 155 galaxies; 141 of these are cluster members within  $2.44 h^{-1}$   $\text{Mpc}$  of the cluster center. The completeness limit of the spectroscopic survey is  $H \sim 13$  ( $M_H \sim M_H^*$ ). The cluster velocity dispersion of  $\sigma \sim 1000$   $\text{km s}^{-1}$  remains constant out to the limiting radius. We find no evidence for substructure in the cluster. The cluster mass within  $R = 2.4 h^{-1}$   $\text{Mpc}$  is  $7.6 \pm 1.3 \times 10^{14} h^{-1} M_\odot$ .

We compute the cluster luminosity function; the Schechter parameters  $\alpha = -1.14 \pm 0.08$  and  $M_H^* = -24.3 \pm 0.2$  (with  $h = 0.5$ ) agree well with other  $H$ -band luminosity functions. From the virial theorem and the caustic method we compute one of the first mass-to-light ratios at  $H$ ; the result is  $M/L_H = 82 - 127h M_\odot/L_\odot$  within  $1.5h^{-1}$   $\text{Mpc}$ . This ratio corresponds to  $374 - 579h M_\odot/L_\odot$  at  $R$ . The agreement of our IR measurement with previous  $M/L$  determinations indicates that at low redshift dust and young stellar populations may produce only negligible systematic errors in optical mass-to-light ratios.

*Subject headings:* galaxies: clusters: individual (A1644) — galaxies: luminosity function, mass function

---

<sup>1</sup>Visiting Astronomer, Cerro Tololo Inter-American Observatory. CTIO is operated by AURA, Inc. under contract to the National Science Foundation.

## 1. INTRODUCTION

Observations of galaxy clusters are a useful tool for constraining models of structure formation and of determining cosmological parameters. Cluster mass-to-light ratios, traditionally measured at optical wavelengths, are important in estimating  $\Omega_0$  (c.f. Bahcall 1977; Bahcall, Lubin, & Dorman 1995; Carlberg et al. 1996; and references therein). The luminosity functions (LFs) of clusters can also be compared to field LFs to investigate the effects of galaxy evolution in the cluster environment.

Infrared observations of clusters have several advantages over optical measurements. IR emission is less affected than visible light by absorption and scattering due to dust, which may be interstellar or intracluster (Zwicky 1962; Boyle, Fong, & Shanks 1988) in origin. Galactic infrared emission is also dominated by the older stellar population and is relatively insensitive to short-lived blue stars and changes in the star formation rate (Bruzual & Charlot 1993). Infrared radiation should therefore be a good tracer of the total stellar mass of the cluster.

Until now, the small fields of view of infrared CCD arrays have impeded deep large-area near-infrared photometry of clusters. For example, Andreon & Pelló (2000) measure the  $H$ -band LF of the Coma cluster to a faint limiting magnitude ( $M_H^* + 6$ ), but in a projected area of 2% of the size of our survey. The 2MASS project surveys the entire sky but is almost 2 mag shallower than our data at  $H$ . Cluster surveys at  $K$  are slightly more common (De Propris et al. 1999; Trentham & Mobasher 1998; Barger et al. 1998), but most suffer from similar limitations.

The  $H$ -band data we discuss here, covering a projected area of  $9 h^{-2}$  Mpc<sup>2</sup> and reaching  $M_H \sim M_H^* + 3$ , make Abell 1644 (A1644) one of the best-studied clusters at near-infrared wavelengths. We constrain the IR LF and compare its shape and parameters to those for other cluster and field surveys. The addition of extensive spectroscopy enables us to comment on several kinematic issues. We examine the properties of emission and absorption galaxies, test for substructure, and compute the infrared mass-to-light ratio of the cluster. This measurement,  $M/L_H \sim 82 - 127 h M_\odot/L_\odot$ , is consistent with observed optical values and is one of the only existing cluster  $M/L$  determinations in the infrared.

In Section 2 we describe our photometric and spectroscopic observations. Section 3 contains an analysis of the kinematic properties of the cluster. In Section 4 we compute the LF and mass-to-light ratio, and we summarize in Section 5.

## 2. OBSERVATIONS

Abell 1644 is a nearby rich cluster with a cD galaxy ( $\alpha = 12^{\text{h}}57^{\text{m}}11^{\text{s}}.6$ ,  $\delta = -17^{\circ}24'34''.4$  J2000,  $cz = 14,233 \pm 33 \text{ km s}^{-1}$ ) at its center. Our  $H$ -band photometric observations cover a  $3 \times 3 h^{-2} \text{ Mpc}^2$  region surrounding the cluster core to limiting  $H \sim 16$ . We also measured redshifts for 155 galaxies within  $2.44 h^{-1} \text{ Mpc}$  of the cluster center. The combined sample of 123 cluster members with both spectral and photometric data is complete to  $H \sim 13$ .

### 2.1. Photometry

We obtained  $H$ -band photometry covering a  $36' \times 36'$  region centered on  $\alpha = 12^{\text{h}}57^{\text{m}}35^{\text{s}}$   $\delta = -17^{\circ}27'21''$  on 1997 April 16-19. We used the CIRIM infrared camera on the 1.5 m telescope at Cerro Tololo Inter-American Observatory (CTIO). The scale for the  $256 \times 256$  array is  $1''.137 \text{ pixel}^{-1}$ , and the duration of each exposure was  $6 \times 10^{\text{s}}$ . We operated the instrument in a mapping mode which acquired pairs of dithered images offset by  $10''$ . We then covered the survey region with a tiling of dithered pairs which overlap by  $40''$ . In addition, we surveyed two off-cluster fields of sizes  $0.22 \text{ deg}^2$  and  $0.04 \text{ deg}^2$  to ascertain background statistics.

On the nights of 1999 April 25-29 and 1999 May 26 we used the Stelircam IR camera on the 1.2 m telescope at Fred L. Whipple Observatory (FLWO) on Mt. Hopkins, Arizona to expand our infrared survey. We operated the  $256 \times 256$  instrument ( $1''.2 \text{ pixel}^{-1}$ ) in a mapping mode similar to that used at CTIO. Of the six nights at FLWO, two were not photometric. On the remaining nights we gathered data over a  $0.99 \text{ deg}^2$  region bordering the CTIO observations (bringing our total coverage in the cluster to  $1.35 \text{ deg}^2$ ), and we increased the sizes of our off-fields to  $0.41 \text{ deg}^2$  and  $0.44 \text{ deg}^2$ . We also imaged a small area in the center of the cluster, overlapping the CTIO data, to assess systematic differences between the two surveys.

For each photometric night, we first used NOAO IRAF<sup>2</sup> commands to flat-field and sky-subtract each frame. We calculated the zero point of each night's magnitude scale by fitting a linear solution to several standard star images and correcting each object frame for airmass. We then used the SExtractor software package for source detection and photometry. In addition to the usual aperture and isophotal magnitudes, SExtractor calculates a composite MAG\_BEST. MAG\_BEST is useful in crowded fields and is equal to the Kron

---

<sup>2</sup>IRAF is distributed by the National Optical Astronomy Observatory, which is operated by the Association of Universities for Research in Astronomy, Inc. under contract to the National Science Foundation.

magnitude (Kron 1980) if no neighbor can bias the Kron aperture magnitude by more than 10%. Otherwise it is the corrected isophotal magnitude (Bertin & Arnouts 1996). We adopt MAG\_BEST for our subsequent data analysis. To demonstrate the consistency of the photometry, we plot the magnitude differences as a function of MAG\_BEST for objects observed in successive dithered frames on 1997 April 17 (Figure 1). The rms error in the photometry is  $\Delta m_{rms} \sim 0.12$  mag at  $H = 16$ .

The SExtractor software also includes an algorithm to separate stars and galaxies based on morphology. Each object identified has a value CLASS\_STAR which ranges from zero for galaxies to one for stars. Ambiguous objects lie somewhere in between. We examine the images manually and find that CLASS\_STAR accurately separates stars and galaxies brighter than  $H \sim 14.5$ ; fainter objects are indistinguishable by eye in these images.

An examination of the CTIO and FLWO data in the overlap region reveals that the seeing is better in the CTIO images. However, there is little systematic difference in the photometry. The average magnitude difference between objects observed at FLWO and CTIO is  $\overline{\Delta m} = 0.04$  mag, and the rms scatter is  $\Delta m_{rms} = 0.15$  mag. The SExtractor star/galaxy separation gives consistent results for objects observed at both sites. In the overlap region, 93% of the objects with  $H < 14.5$  identified as galaxies in the FLWO data are also classified as galaxies in the CTIO data.

Table 1 shows photometric data for the 861 galaxies in our infrared survey. For  $H < 13$  the galaxy spectroscopic survey is complete; for  $13 < H < 16$  we list all objects with CLASS\_STAR  $< 0.5$ . Columns (1) and (2) give the right ascension and declination of each galaxy; column (3), the apparent  $H$  magnitude (MAG\_BEST); and column (4), the redshift if measured.

## 2.2. Spectroscopy

We acquired optical spectra for 155 galaxies in the region of Abell 1644 during 2000 January-June with FAST, a high throughput slit spectrometer mounted on the 1.5 m telescope at FLWO. The FAST setup includes a 300 groove  $\text{mm}^{-1}$  grating and 3" slit, and yields spectra which cover 3600-7600Å at a resolution of  $\sim 6\text{Å}$ . Although Dressler & Sackett (1988a, hereafter DS) measured 103 redshifts in the region of Abell 1644, we re-acquired spectra of 91 of their objects to assure uniformity throughout our data set and to assess the spectral type of the galaxies. The remaining twelve DS galaxies are either too faint for FAST redshift measurements or are outside our survey region. We selected 64 additional targets on the basis of the DS catalog, digitized sky survey images, and our own infrared survey.

We obtained a reduced spectrum for each object using IRAF. We made bias, flat-field, and illumination corrections to each frame and then used the IRAF XCSAO task to obtain redshifts via cross-correlation with standard emission and absorption templates. The resulting spectroscopic sample is complete to  $H \sim 13$  in the region where we have  $H$ -band photometry. We tested the differences between the FAST and DS observations for the 91 common galaxies. The FAST velocities are systematically lower by  $\sim 39 \text{ km s}^{-1}$ , and the rms velocity difference is  $\Delta v_{rms} = 80 \text{ km s}^{-1}$ . These offsets are consistent with the estimated velocity errors of roughly  $30 \text{ km s}^{-1}$  (FAST) and  $45 \text{ km s}^{-1}$  (DS).

Table 2 lists properties of the 155 galaxies with measured redshifts. Columns (1) and (2) give the right ascension and declination; column (3), the radial velocity; column (4), the error on the radial velocity; column (5), the spectral type (either emission or absorption as discussed in Section 3.1); column (6), MAG\_BEST (if available); and column (7), the reference number from the DS catalog for galaxies in the DS list.

### 2.3. Cluster Sample

Figure 2a shows the measured velocity distribution. A1644 is remarkably isolated in redshift space. A few background galaxies are visible at redshifts up to  $cz \sim 65,000 \text{ km s}^{-1}$ . There is also evidence of foreground structure in the range  $2500 < cz < 10,000 \text{ km s}^{-1}$ . Figure 2b shows the 141 cluster members with redshifts between  $10,000$  and  $20,000 \text{ km s}^{-1}$ .

The mean radial velocity of the cluster is  $c\bar{z} = 14,295 \pm 93 \text{ km s}^{-1}$  with a dispersion of  $\sigma = 1108_{-61}^{+73} \text{ km s}^{-1}$ , computed at the 68% confidence limit as in Danese, De Zotti, & di Tullio (1980). The radial velocity of the cD ( $14,233 \pm 33 \text{ km s}^{-1}$ ) is coincident with the overall cluster mean. The cluster sample is isolated from foreground and background galaxies by velocity gaps of  $3244 \text{ km s}^{-1}$  on the low end and  $4589 \text{ km s}^{-1}$  on the high end. The sizes of these gaps are  $2.9\sigma$  and  $4.1\sigma$ , respectively. There are 123 cluster members within the region of infrared photometry; Figure 2c shows the velocity distribution of these galaxies.

## 3. KINEMATICS

### 3.1. Emission and Absorption Galaxies

We separate the galaxies into emission (Em) and absorption (Abs) systems. Emission galaxies are those objects with a larger R value when cross-correlated with the emission template; all other galaxies are classified as absorption. Figure 3 shows the positions of the

141 cluster members according to spectral type. There are 18 emission and 123 absorption systems. The absorption galaxies are more centrally condensed; the median projected distances of the Abs and Em samples from the cD galaxy are 20'.1 and 27'.5, respectively. This difference is only marginally statistically significant; a rank-sum test applied to the two samples gives a 97% confidence that the Em and Abs systems do not come from the same parent spatial distribution.

Figure 4 shows the radial velocity distributions of the Abs and Em samples. The absorption galaxies have  $c\bar{z} = 14,363 \pm 98 \text{ km s}^{-1}$  and  $\sigma = 1095^{+77}_{-64} \text{ km s}^{-1}$ . The dispersion of the Em sample ( $\sigma = 1123^{+268}_{-156} \text{ km s}^{-1}$ ) is comparable, but the mean velocity of  $c\bar{z} = 13,800 \pm 273 \text{ km s}^{-1}$  is lower. However, a rank-sum test gives only a 96% confidence that the Em and Abs galaxies follow different velocity distributions.

### 3.2. Substructure

Dressler & Shectman (1988b) define a test parameter  $\delta$  which measures the deviation of a subgroup's local mean velocity and dispersion,  $\bar{v}_{local}$  and  $\sigma_{local}$ , from that of the cluster's overall values ( $\bar{v}$  and  $\sigma$ ):

$$\delta^2 = \frac{n}{\sigma^2} [(\bar{v}_{local} - \bar{v})^2 + (\sigma_{local} - \sigma)^2], \quad (1)$$

where  $n$  is the number of galaxies in the subgroup. The cumulative deviation is  $\Delta = \sum_{i=1}^N \delta_i$ , where  $N$  is the number of cluster members and for each galaxy we calculate  $\delta_i$  using the galaxy and its  $n-1$  nearest neighbors. For a Gaussian velocity distribution with only random fluctuations,  $\Delta \sim N$ ; the presence of substructure can cause  $\Delta$  to be significantly higher than  $N$ .

Dressler & Shectman (1988b) analyze 92 members of A1644 with  $n = 11$  and find evidence for substructure in the southeastern quadrant of the cluster. To test the significance of this structure, Dressler and Shectman randomly shuffle the velocities of the galaxies to create roughly 1000 model clusters. They calculate the value of  $\Delta$  for each model and find that only 2.7% of the Monte Carlo clusters have  $\Delta \geq \Delta_{observed}$ .

We duplicate the Dressler and Shectman analysis for our larger sample of 141 cluster members. Allowing  $n$  to range from five to 105, we calculate the  $\Delta$  statistic for each subgroup size. We also create 5000 Monte Carlo models for each value of  $n$  and compute the probability that  $\Delta \geq \Delta_{observed}$ . Figure 5 shows the results.

With  $n = 11$ , we find that  $\Delta$  is greater than or equal to  $\Delta_{observed}$  in 17.5% of the simulated clusters. Thus our larger sample, when compared to the Dressler and Shectman

catalog, no longer provides evidence for substructure on this scale. The best evidence for substructure occurs with  $n = 6$  and  $n = 67$ . However, these detections are not statistically significant, with probabilities of  $\Delta \geq \Delta_{\text{observed}}$  of 4.3% and 5.0%, respectively.

### 3.3. Velocity Dispersion Profile

Figure 6 shows an azimuthally averaged radial profile of the cluster velocity distribution for both Abs and Em galaxies. We compute the velocity dispersion of the cluster as a function of distance from the cD galaxy and plot the results in Figure 7. We choose the cD as the geometric center of the cluster because of the lack of evidence for substructure. Moving outward from the cD, we calculate the velocity dispersion of successive groups of 11 galaxies arranged in order of increasing radius. The error bars in the plot represent the 68% confidence level for uncorrelated points.

The velocity dispersion of the cluster remains roughly constant for  $R \lesssim 1.9h^{-1}$  Mpc; at this radius it nearly doubles. The increase at large radius is extremely sensitive to the presence of three high-velocity galaxies circled in Figure 6. When we exclude these galaxies (Figure 7, bottom plot) the velocity dispersion at  $R \sim 1.9 h^{-1}$  Mpc decreases by a factor of three. We suggest that the three high-velocity galaxies may be outliers and that  $\sigma$  is roughly constant as a function of radius. Treating these objects as background is consistent with the results of our caustic analysis (Section 3.4), and also with Dressler & Shectman (1988b), who select  $cz \lesssim 18,000 \text{ km s}^{-1}$  as a criterion for membership in A1644.

### 3.4. Cluster Mass

We calculate the mass of A1644 in two ways. Our first mass estimate depends on the “caustic” technique of Diaferio & Geller (1997). A hierarchical clustering model predicts the existence of two caustic curves with amplitude  $A(R)$  approximately equal to the escape velocity from the cluster at radius  $R$ . Diaferio (1999) shows that  $A(R)$  is related to the mass of the cluster interior to  $R$ :

$$GM_{est}(< R) = \frac{1}{2} \int_0^R A^2(x) dx. \quad (2)$$

We use the techniques of Diaferio (1999) with smoothing parameter  $q = 25$  to calculate the caustics of A1644 (Figure 8). Of the 141 presumed cluster members, 127 lie within the caustics; the fourteen remaining galaxies may in fact be outliers. Equation 2 automatically excludes these outliers from the caustic mass determination.

Our second mass estimate uses a virial estimator (Binney & Tremaine 1987):

$$M_{est} = \frac{3\pi N}{2G} \frac{\sum_{i=1}^N v_{p,i}^2}{\sum_{i=1}^N \sum_{j<i} |R_i - R_j|^{-1}}, \quad (3)$$

where  $v_{p,i}$  is the radial velocity of each galaxy with respect to the cluster mean and  $R_i$  is the galaxy's position relative to the cD. This estimator assumes that the galaxies are embedded in a diffuse dark matter distribution, and that the spatial arrangement of galaxies traces the dark matter.

The virial mass is very sensitive to outliers. In Figure 9 we first plot  $M_{virial}$  using the 141 galaxies with  $10,000 \text{ km s}^{-1} < cz < 20,000 \text{ km s}^{-1}$ . The virial mass decreases by a factor of two or more, even at large radius, when we include only those galaxies which lie inside the caustics. For comparison, we plot  $M_{caustic}$  for three different values of the smoothing parameter; the caustic mass is much more robust.

Equation 3 overestimates the true value of  $M$  because we have not subtracted the virial surface term (The & White 1986). When the surface term  $C(r)$  is included, the corrected virial mass is

$$M_{cv}(< b) = M_{est} \{1 - C(b)\} = M_{est} \left\{ 1 - 4\pi b^3 \frac{\rho(b)}{\int_0^b 4\pi r^2 \rho(r) dr} \left[ \frac{\sigma_r(b)}{\sigma(< b)} \right]^2 \right\}, \quad (4)$$

where  $\rho(r)$  is the radial density distribution,  $\sigma_r$  is the radial component of the velocity dispersion, and  $\sigma(< b)$  is the integrated velocity dispersion within the limiting radius  $b$  (Girardi et al. 1998).

Calculation of the surface term requires knowledge of both the velocity dispersion profile and the density distribution. While  $\sigma(r)$  can be constrained from the data, the density profile is unknown and is, in fact, the very quantity we are attempting to correct via equation 4. To approximate  $\rho(r)$  we fit a Navarro, Frenk, & White (1995, 1996, 1997, hereafter NFW) mass profile to  $M_{caustic}$ . The NFW functional forms of the mass and density profiles are

$$M(< r) = 4\pi\delta_c\rho_c r_c^3 \left[ \log(1 + r/r_c) - \frac{r/r_c}{1 + r/r_c} \right] \quad (5)$$

and

$$\rho(r) = \frac{\delta_c\rho_c}{(r/r_c)(1 + r/r_c)^2}, \quad (6)$$

where  $\delta_c$  and  $r_c$  are model parameters and  $\rho_c$  is the critical density of the universe. We fit equation 5 to the caustic mass profile and substitute the best-fit parameters into equation 6 to recover the density distribution. We then use the fitted  $\rho(r)$  to estimate the virial surface term via equation 4.



To estimate  $C(r)$  one must also assume a value of the anisotropy parameter  $\beta(r) = 1 - \sigma_\theta^2/\sigma_r^2$ . Girardi et al. (1998) show that clusters with a flat velocity dispersion profile are best described by models with  $\beta(r) = 0$ . We adopt this value of  $\beta(r)$  and compute the virial surface term. The overall trend of the surface term is decreasing with radius. However,  $C(r)$  fluctuates on small scales because of its dependence on  $\sigma(r)$ . At  $r = 1.5 h^{-1}$  Mpc,  $C(r) \sim 0.2 \pm 0.1$ .

We use a statistical “jackknife” procedure (Diaconis & Efron 1983) to calculate errors in the virial mass,  $\Delta M/M \sim 2 - 4\%$  for  $R = 0.5 - 1.5 h^{-1}$  Mpc. Systematic sources of error in the virial mass dwarf this formal jackknife estimate; the surface term correction is highly uncertain due to the assumptions regarding  $\rho(r)$  and  $\beta(r)$ . In addition, the virial estimate depends strongly on the particular galaxy sample.

Figure 10 shows our final estimates of the caustic and virial mass profiles. For consistency, we base both estimates on the same set of 127 galaxies enclosed by the caustics. Errors in  $M_{caustic}$  represent uncertainty in the location of the caustics. The virial mass incorporates the surface term correction. We show  $M_{virial}$  as an envelope whose maximum and minimum values signify the range of masses consistent with the jackknife errors and the uncertainty in  $C(r)$ . With our adopted errors, the caustic and virial mass estimators are consistent at the  $2\sigma$  level at all radii.

Figure 10 also includes two X-ray mass determinations from Ettori, Fabian, & White (1997). They arrive at mass estimates for A1644 based on *Einstein Observatory* IPC X-ray data. Their deprojection analysis yields  $M_{dpr} = 1.05 \times 10^{14} h^{-1} M_\odot$  within  $0.305 h^{-1}$  Mpc. They then extrapolate the deprojection mass to  $R_{500}$ , the radius where  $\rho/\rho_{crit} = 500$ ; the extrapolated mass is  $M_{500} = 4.06 \times 10^{14} h^{-1} M_\odot$  within  $0.85 h^{-1}$  Mpc. Our caustic mass estimate is consistent with the X-ray data at both radii.

## 4. PHOTOMETRIC PROPERTIES

### 4.1. Luminosity Function

Figure 11 shows the differential  $H$ -band luminosity function of A1644. In the bins with complete spectroscopy ( $H < 13$ ) redshifts determine cluster membership. At the faint end we estimate the number of field galaxies because we do not have spectra. We model the number of field galaxies in each magnitude bin by a power law of the form

$$N(m_1 < m < m_2) = C \int_{m_1}^{m_2} 10^{0.67m} dm, \quad (7)$$

where  $C$  is a normalization constant. We assume the background slope of 0.67 determined by Gardner, Cowie, & Wainscoat (1993) from a compilation of  $K$ -band field surveys. As our best estimate of the background, we normalize the power law by integrating equation 7 from  $H = -\infty$  to  $H = 14$  and equating the left hand side with the number of field galaxies in the direction of the cluster; there are  $5 \pm 2$  field galaxies  $\text{deg}^{-2}$  with  $H < 14$  in our photometric region. Our off-cluster survey contains  $39 \pm 6$  bright galaxies per square degree, and Gardner et al. (1993) and Szokoly et al. (1998) observe roughly  $13 \pm 3$  and  $23 \pm 6$  galaxies  $\text{deg}^{-2}$  in this magnitude range. Although these field counts are statistically consistent with our estimate, the large variations in the normalization can produce a rising, flat, or declining faint end of the A1644 cluster LF.

After subtracting the background fit normalized by our redshift survey from the total number of faint galaxies identified by the SExtractor CLASS\_STAR parameter, we characterize the data with a Schechter luminosity function. We fit to the Schechter (1976) form of the luminosity function

$$n_e(L)dL = n^*(L/L^*)^\alpha \exp(-L/L^*)d(L/L^*), \quad (8)$$

where  $\alpha$  is the faint-end slope,  $L^*$  is a characteristic luminosity, and  $n^*$  is a normalization constant. In terms of absolute magnitude  $M$  the luminosity function is

$$N_e(M)dM = k n^* \exp\{-k(\alpha + 1)(M - M^*)\} - \exp[-k(M - M^*)]dM, \quad (9)$$

where  $k \equiv (\ln 10/2.5)$  and  $M^*$  is the absolute magnitude corresponding to  $L^*$  (Kashikawa et al. 1995). At the mean redshift of our cluster  $M_H = m_H - 35.78 + 5 \log h$ .

We fit a Schechter function to our data by minimizing the quantity

$$\chi^2 \equiv \sum \frac{[N(M_i) - N_e(M_i)]^2}{\sigma_i^2}, \quad (10)$$

where  $N(M_i)$  and  $N_e(M_i)$  are the observed and fitted numbers of galaxies in the  $i$ th magnitude bin and  $\sigma_i$  is the variance in the  $i$ th measurement. With respect to the maximum likelihood method (Sandage, Tammann, & Yahil 1979), also commonly used to fit luminosity functions, a  $\chi^2$  fit has the disadvantage that the data must be binned, but it is advantageous because it provides a measure of the goodness of the fit. We assume a Poissonian variance in the total number of galaxies and in the number of background galaxies in each bin.

We determine the best-fit Schechter function (solid curve in Figure 11); the best-fit parameters are  $\alpha = -1.14 \pm 0.08$ ,  $M^* = -24.3 \pm 0.2$ , and  $n^* = 114 \pm 22$  (here and in subsequent discussions of absolute magnitudes we take  $h = 0.5$ ). The Schechter function is a good fit to the faint end of the LF and slightly underpredicts the number of bright galaxies. The minimum value of  $\chi^2$  is 6.3 with 8 degrees of freedom.

Our best-fit values of  $\alpha$  and  $M_H^*$  are in good agreement with a survey of A1644 in the visible (Kashikawa et al. 1995). They fit a Schechter LF (with  $\alpha$  fixed at -1.25) to the  $R$ -band luminosity distribution and find  $M_R^* = -21.50$ . With an expected elliptical color of  $(R - H) \sim 2.5$ , the characteristic magnitude at  $H$  is  $M_H^* \sim -24.0$ , which agrees very well with our measurement.

There are several  $K$ -band field luminosity functions. Parameters derived from these surveys span roughly  $-1.0 < \alpha < -1.3$  and  $-25.1 < M_K^* < -23.6$  (Mobasher, Sharples, & Ellis 1993; Szokoly et al. 1998; Loveday 2000). Our values for A1644 are consistent with this range, assuming  $H - K = 0.25$  as above. Parameters derived from  $K$ -band studies of clusters are similar. De Propris et al. (1999) find  $M_K^* \sim -24.9 \pm 0.5$  with  $\alpha$  fixed at -0.9 for clusters in their  $z = 0.15$  bin. A separate survey of five X-ray luminous clusters finds a composite  $\alpha = -1.38 \pm 0.24$  (Trentham & Mobasher 1998). Our results are consistent with these low  $z$  counts for typical early-type galaxy color, but not with Barger et al. (1998), who find an average  $M_K^* = -25.4 \pm 0.1$  for 10 clusters with  $0.31 < z < 0.56$ . The discrepancy could be due to luminosity evolution, although Barger et al. claim that their  $M_K^*$  is not significantly brighter than the  $z \sim 0$  values.

At  $H$  fewer data are available. An  $H$ -band study of a  $0.1 \text{ deg}^2$  region of the Coma cluster finds  $\alpha = -1.3 \pm 0.2$  and  $M_H^* = -24.6 \pm 1.0$ , with a dip in the LF at  $M_H = -22.2$  ( $H \sim 13.5$ ) (Andreon & Pelló 2000). We estimate the errors on their values of  $\alpha$  and  $M_H^*$  by examining the 68% confidence contours in their Figure 3. An imaging study of A548 over a much larger area ( $0.9 \text{ deg}^2$ ) reveals a similar dip at  $H \sim 13 - 13.5$  (S. J. Kenyon et al., in preparation). The number of galaxies in our survey is too small to evaluate the presence of a dip at  $H \sim 13.5$ . The counts in the  $13 < H < 13.5$  and  $13.5 < H < 14$  bins ( $55 \pm 7$  and  $68 \pm 8$ , respectively) are very similar; the LF in this region is thus consistent with either a flat, rising, or declining slope.

## 4.2. Mass-to-Light Ratio

We determine the total  $H$ -band luminosity of A1644 by extrapolating the luminosity function. For a magnitude-limited survey described by a Schechter function the observed fraction of the total light is given by  $\Gamma(\alpha + 2, L_{min}/L^*)/\Gamma(\alpha + 2)$ , where  $\Gamma(x, y)$  is the incomplete Gamma function and  $L_{min}$  and  $L^*$  are the luminosities corresponding to the completeness limit and  $M^*$ . With a completeness limit of  $H = 16$ , the fitted Schechter parameters imply that we observe 90.6% of the total light. Our photometric survey covers a square field  $9 h^{-2} \text{ Mpc}^2$  in area. The photometry is therefore complete within  $0.5(9 h^{-2} \text{ Mpc}^2)^{1/2} = 1.5 h^{-1} \text{ Mpc}$  of the center of the field. Inside this radius the total luminosity

is  $L_H = 7.6 \pm 0.4 \times 10^{12} h^{-2} L_\odot$ ; the quoted error in  $L_H$  reflects the uncertainty in the LF parameters.

For comparison, we integrate the visible LF in a smaller  $0.82 \text{ deg}^2$  region of A1644 (Kashikawa et al. 1995). Using their values of  $\alpha$ ,  $M_R^*$ , and  $M_R^{lim}$ , the total  $R$ -band light within  $1.1 h^{-1} \text{ Mpc}$  is  $L_R \sim 1.1 \times 10^{12} h^{-2} L_\odot$ . Within the same radius we compute the  $H$ -band luminosity and use typical galactic colors and  $(R-H)_\odot = 0.85$  to convert  $H$  photometry to  $R$ . The result is  $L_H = 5.1 \pm 0.3 \times 10^{12} h^{-2} L_\odot$  which implies  $L_R \sim 1.12 \pm 0.06 \times 10^{12} h^{-2} L_\odot$ , in excellent agreement with Kashikawa et al. The agreement implies that the optical luminosity of A1644 is only slightly affected by factors such as dust extinction and recent star formation activity.

Figure 12 shows the radial  $M/L_H$  profile. The mass-to-light ratio is flat for  $R \gtrsim 0.4 h^{-1} \text{ Mpc}$ , suggesting that the dark matter fraction is constant outside this radius. The increased  $M/L$  at  $R \lesssim 0.35 h^{-1} \text{ Mpc}$  is a result of a depressed luminosity near the cluster core. At the limiting photometric radius of  $1.5 h^{-1} \text{ Mpc}$  the caustic and virial mass-to-light ratios are  $M/L_H = 82 \pm 13 h M_\odot/L_\odot$  and  $M/L_H = 127 \pm 26 h M_\odot/L_\odot$ .

For A1644, Girardi et al. (2000) obtain  $M/L_{B_j} \sim 250 h M_\odot/L_\odot$  within  $1.5 h^{-1} \text{ Mpc}$ . Transforming from  $B_j$  to  $H$  gives  $M/L_H \sim 40 h M_\odot/L_\odot$  for their data. This value is roughly half of our caustic estimate. Because our measured masses are almost exactly the same, the difference in  $M/L$  is due to their larger luminosity. Our luminosity determination is based on CCD photometry and agrees well with the optical CCD photometry of Kashikawa et al. (1995); Girardi et al.’s analysis is based on digitized and calibrated survey plates from the COSMOS/UKST Southern Sky Object Catalog and is discrepant with Kashikawa et al.

Cluster mass-to-light determinations at  $H$  are scarce. We thus transform to  $R$  and  $V$  using the  $R-H$  colors above along with  $V-H \sim 3$  for early-type galaxies and  $(V-H)_\odot = 1.37$ . The mass-to-light ratios within  $1.5 h^{-1} \text{ Mpc}$  are then equivalent to:

$$M_{caustic}/L_R = 374 \pm 59 h M_\odot/L_\odot$$

$$M_{caustic}/L_V = 369 \pm 59 h M_\odot/L_\odot.$$

$$M_{virial}/L_R = 579 \pm 119 h M_\odot/L_\odot$$

$$M_{virial}/L_V = 572 \pm 117 h M_\odot/L_\odot$$

The caustic mass-to-light ratio is consistent with most previous measurements of cluster  $M/L$  ratios; typical values using virial masses are  $M/L_R \sim 300 h M_\odot/L_\odot$  (Carlberg et al. 1996; Girardi et al. 2000), with a range of  $200 - 600 h M_\odot/L_{\odot,R}$  (Dressler 1978). Our virial  $M/L$  determination is consistent with the high end of this range. Estimates of  $M/L$  using

X-ray masses tend to be somewhat lower. Hradecky et al. (2000) find  $M/L_V = 154 - 468 h$  solar units for seven nearby Abell clusters and one group, and *ROSAT* observations of eleven groups and clusters yield  $M/L_V = 200 - 300 h M_\odot/L_\odot$  (David, Jones, & Forman 1995).

## 5. DISCUSSION AND SUMMARY

We discuss a large, deep imaging survey of a galaxy cluster in the near-infrared, covering a  $1.35 \text{ deg}^2$  ( $9 h^{-2} \text{ Mpc}^2$ ) region of A1644. These data allow us to determine the IR LF at  $H$  to roughly  $M_H^* + 3$ , deeper than most previous infrared surveys of comparable size. We also acquired spectra for 155 galaxies (including  $\sim 141$  cluster members) and use these to compute  $M/L_H$  for the cluster. The results are:

1. A grouping of cluster members by spectral type reveals evidence at the 96-97% confidence level for the segregation of emission and absorption galaxies by both velocity and core radius. Although only marginally statistically significant, these detections of segregation with respect to spectral type are in the same direction as the morphological segregation observed in other clusters (Adami, Biviano, & Mazure 1998; Melnick & Sargent 1977; Biviano et al. 1992). In contrast with an earlier analysis by Dressler & Shectman (1988b), there is no significant evidence for substructure on any scale. Our 50% larger sample of cluster members is responsible for the difference.
2. The velocity dispersion of the cluster varies little with radius for  $R \leq 1.5 h^{-1} \text{ Mpc}$ . Near the center,  $\sigma$  is slightly larger than at the periphery, provided that we exclude three high-velocity galaxies at large clustercentric distance which may be background.
3. The luminosity distribution is well-fit by a Schechter function with  $\alpha = -1.14 \pm 0.08$  and  $M_H^* = -24.3 \pm 0.2$ . These parameters agree with previous infrared LF measurements of clusters and field galaxies. In particular, an  $H$ -band determination of the Coma LF (Andreon & Pelló 2000) yields an identical slope and characteristic magnitude to within the errors. The shape of the A1644 LF is consistent with several infrared cluster LFs (Trentham & Mobasher 1998; Barger et al. 1998; De Propris et al. 1999). However, due to small number statistics and the relatively flat slope of the LF at  $H \sim 13 - 13.5$  we are unable to rule out the presence of a dip similar to the ones observed in optical and infrared cluster LFs (Koranyi et al. 1998; Andreon & Pelló 2000).
4. We compute dynamical masses of A1644 based on the virial theorem and on the use of caustics. The caustic technique yields masses which have smaller errors, are more robust, and agree better with X-ray data. These masses, combined with the  $H$ -band

photometry, yield an  $M/L_H \sim 82 - 127 h M_\odot/L_\odot$  within  $R = 1.5 h^{-1}$  Mpc. This mass-to-light ratio is one of the first determinations in the infrared, and corresponds to  $\sim 374 - 579 h M_\odot/L_\odot$  at visible wavelengths. That the infrared  $M/L$  agrees with previous optical determinations suggests that in some clusters biases by factors such as dust and short-lived star formation events are a small effect compared with the errors in the determination of mass-to-light ratios.

We thank the staff members of FLWO and CTIO for assistance with our observations. In particular, Mercedes Gómez assisted with the observations at CTIO, and the remote observers at Whipple Observatory obtained all of the redshifts listed in Table 2. We are grateful to Susan Tokarz for reducing the FAST spectra. We also thank the referee for comments which increased the clarity of the paper.

## REFERENCES

- Adami, C., Biviano, A., & Mazure, A. 1998, *A&A*, 331, 439
- Andreon, S., & Pelló, R. 2000, *A&A*, 353, 479
- Bahcall, N. A. 1977, *ARA&A*, 15, 505
- Bahcall, N. A., Lubin, L. M., & Dorman, V. 1995, *ApJ*, 447, 81
- Barger, A. J., et al. 1998, *ApJ*, 501, 522
- Bertin, E., & Arnouts, S. 1996, *A&AS*, 117, 393
- Binney, J., & Tremaine, S. 1987, *Galactic Dynamics* (Princeton: Princeton University Press)
- Biviano, A., Girardi, M., Giuricin, G., Mardirossian, F., & Mezzetti, M. 1992, *ApJ*, 396, 35
- Boyle, B. J., Fong, R., & Shanks, T. 1988, *MNRAS*, 231, 897
- Bruzual, G., & Charlot, S. 1993, *ApJ*, 405, 538
- Carlberg, R. G., Yee, H. K. C., Ellingson, E., Abraham, R., Gravel, P., Morris, S., & Pritchet, C. J. 1996, *ApJ*, 462, 32
- Danese, L., De Zotti, G., & di Tullio, G. 1980, *A&A*, 82, 322
- David, L. P., Jones, C., & Forman, W. 1995, *ApJ*, 445, 578
- De Propris, R., Stanford, S. A., Eisenhardt, P. R., Dickinson, M., & Elston, R. 1999, *AJ*, 118, 719
- Diaconis, P., & Efron, B. 1983, *Sci. Am.*, 248, 116
- Diaferio, A. 1999, *MNRAS*, 309, 610
- Diaferio, A., & Geller, M. J. 1997, *ApJ*, 481, 633
- Dressler, A. 1978, *ApJ*, 223, 765
- Dressler, A. & Shectman, S. A. 1988a, *AJ*, 95, 284 (DS)
- Dressler, A. & Shectman, S. A. 1988b, *AJ*, 95, 985
- Ettori, S., Fabian, A. C., & White, D. A. 1997, *MNRAS*, 289, 787
- Gardner, J. P., Cowie, L. L., & Wainscoat, R. J. 1993, *ApJ*, 415, L9

- Girardi, M., Borgani, S., Giuricin, G., Mardirossian, F., & Mezzetti, M. 2000, *ApJ*, 530, 62
- Girardi, M., Giuricin, G., Mardirossian, F., Mezzetti, M., & Boschin, W. 1998, *ApJ*, 505, 74
- Hradecky, V., Jones, C., Donnelly, R. H., Djorgovski, S. G., Gal, R. R., & Odewahn, S. C. 2000, *ApJ*, 543, 521
- Kashikawa, N., Shimasaku, K., Yagi, M., Yasuda, N., Doi, M., Okamura, S., & Sekiguchi, M. 1995, *ApJ*, 452, L99
- Koranyi, D. M., Geller, M. J., Mohr, J. J., & Wegner, G. 1998, *AJ*, 116, 2108
- Kron, R.G. 1980, *ApJS*, 43, 305
- Loveday, J. 2000, *MNRAS*, 312, 557
- Melnick, J., & Sargent, W. L. W. 1977, *ApJ*, 215, 401
- Mobasher, B., Sharples, R. M., & Ellis, R. S. 1993, *MNRAS*, 263, 560
- Navarro, J. F., Frenk, C. S., & White, S. D. M. 1995, *MNRAS*, 275, 720
- Navarro, J. F., Frenk, C. S., & White, S. D. M. 1996, *ApJ*, 462, 563
- Navarro, J. F., Frenk, C. S., & White, S. D. M. 1997, *ApJ*, 490, 493
- Sandage, A., Tammann, G. A., & Yahil, A. 1979, *ApJ*, 232, 352
- Schechter, P. 1976, *AJ*, 203, 297
- Szokoly, G. P., Subbarao, M. U., Connolly, A. J., & Mobasher, B. 1998, *ApJ*, 492, 452
- The, L. S., & White, S. D. M. 1986, *AJ*, 92, 1248
- Trentham, N., & Mobasher, B. 1998, *MNRAS*, 299, 488
- Zwicky, F. 1962, in *Problems of Extragalactic Research*, ed. G. C. McVittie (New York: Macmillan), 149



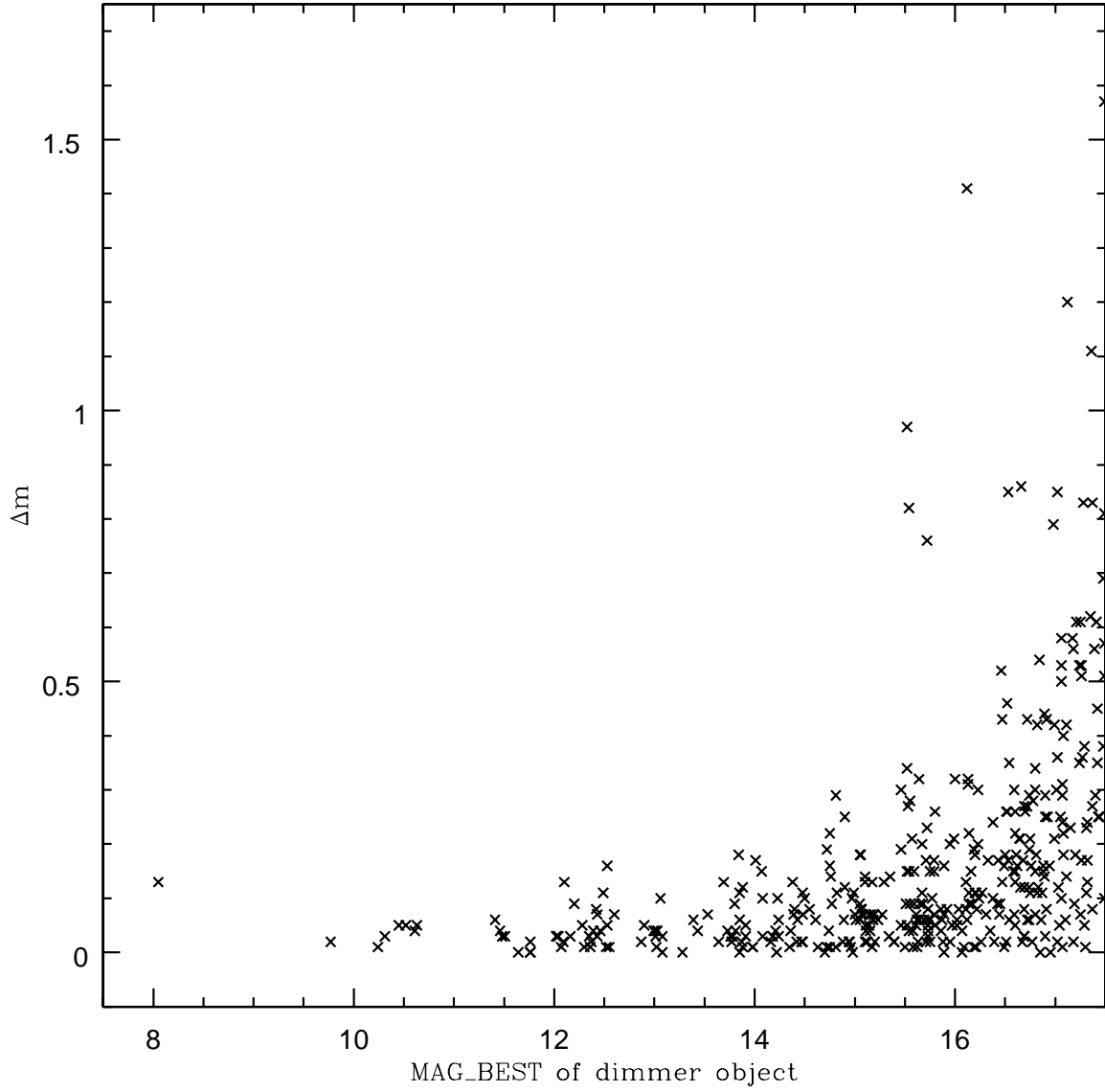


Fig. 1.— Magnitude difference versus dimmer magnitude for objects observed in two successive dithered frames on 1997 April 17. At MAG\_BEST  $\sim$  16 the rms magnitude difference is 0.12 mag.

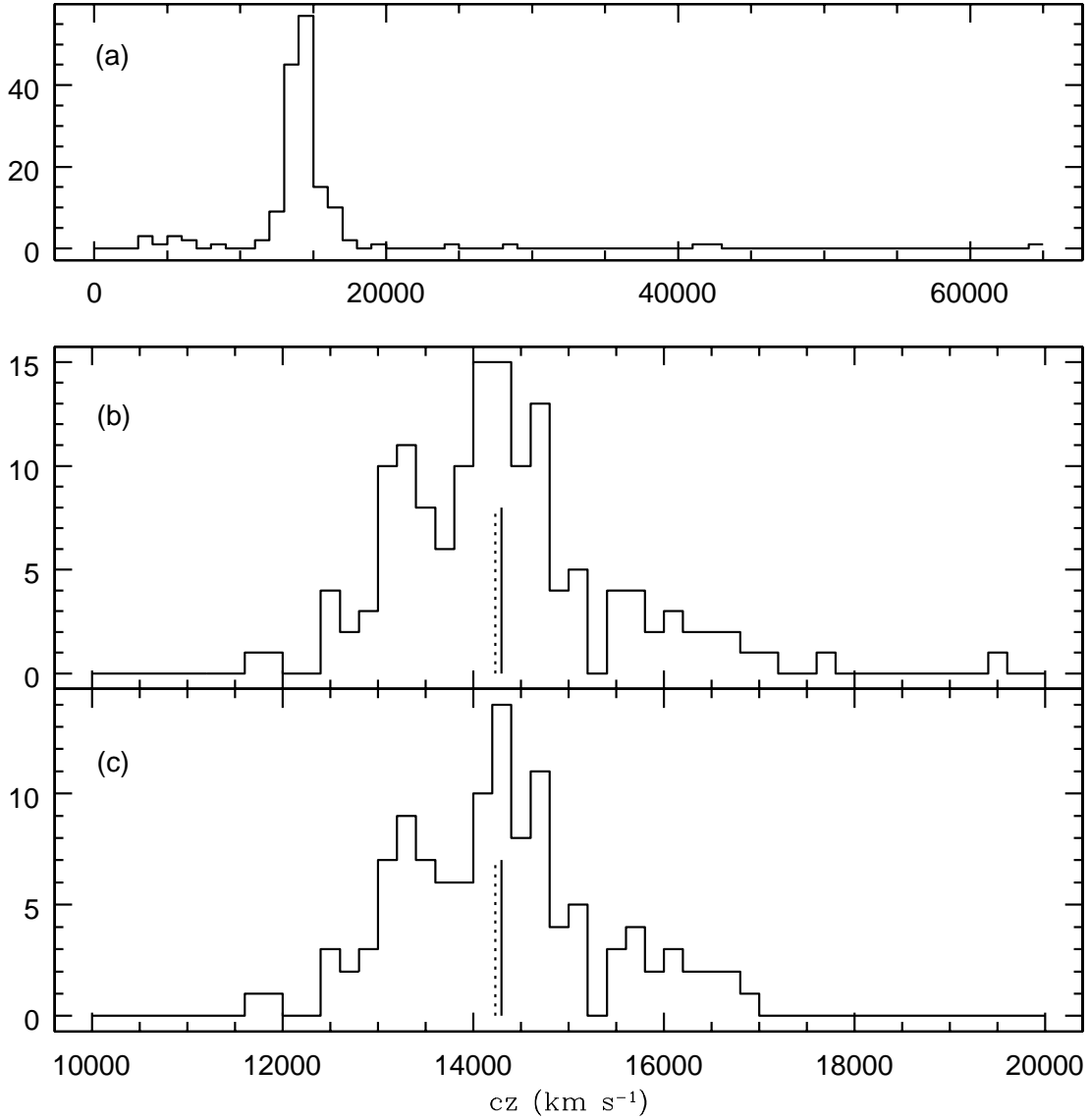


Fig. 2.— a) Velocity distribution of all 155 galaxies observed with FAST. b) Cluster sample of 141 galaxies in the range  $10,000 < cz < 20,000 \text{ km s}^{-1}$ . c) 123 cluster members for which *H*-band photometry is available. In the bottom two plots, the dotted vertical line is the velocity of the cD while the solid line is the mean radial velocity of the cluster.

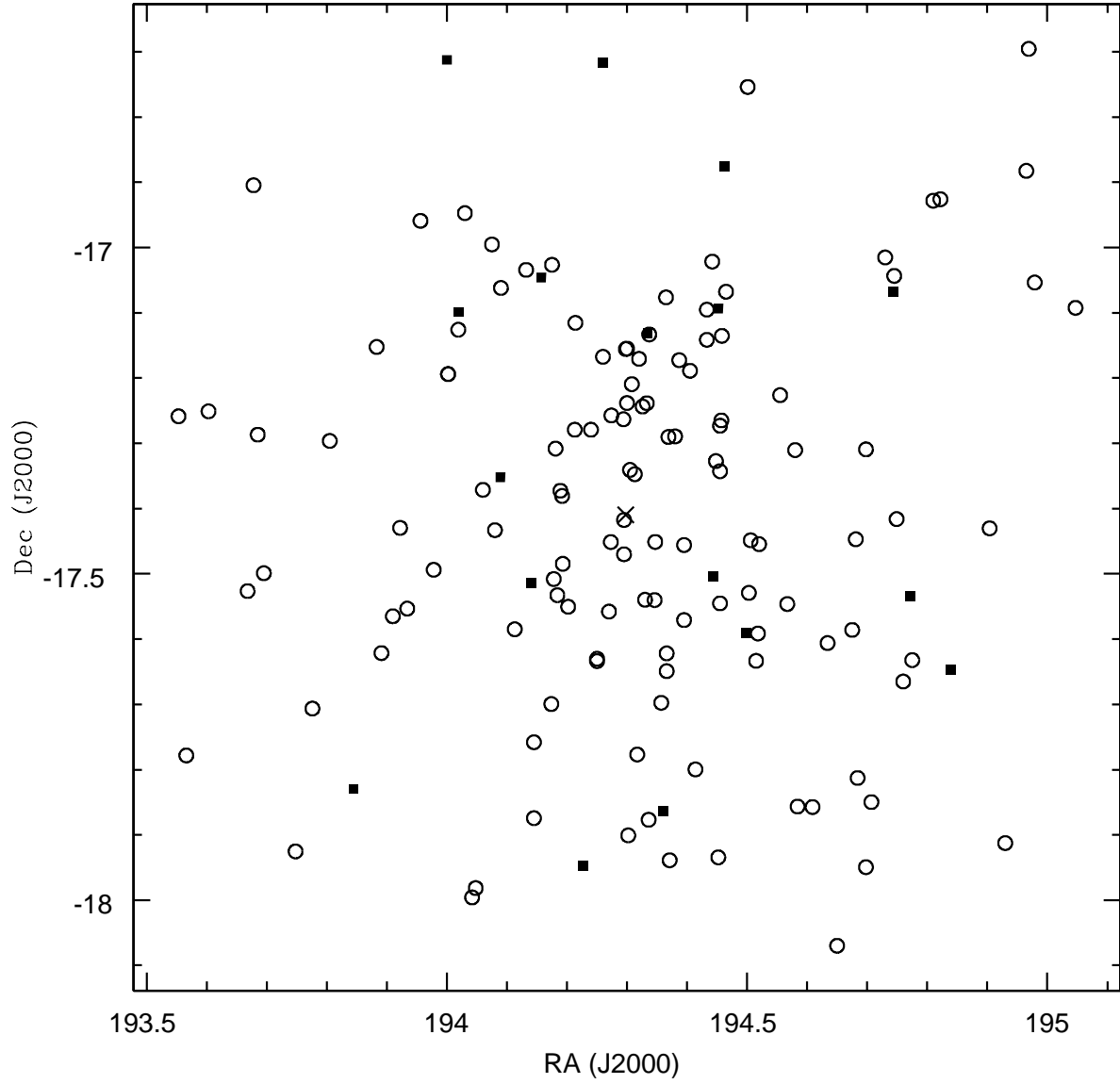


Fig. 3.— Sky positions of the 141 cluster members. Right ascension and declination are in decimal degrees. Open circles represent Abs galaxies and filled squares show Em systems. The cD, an absorption galaxy, is indicated by a cross.

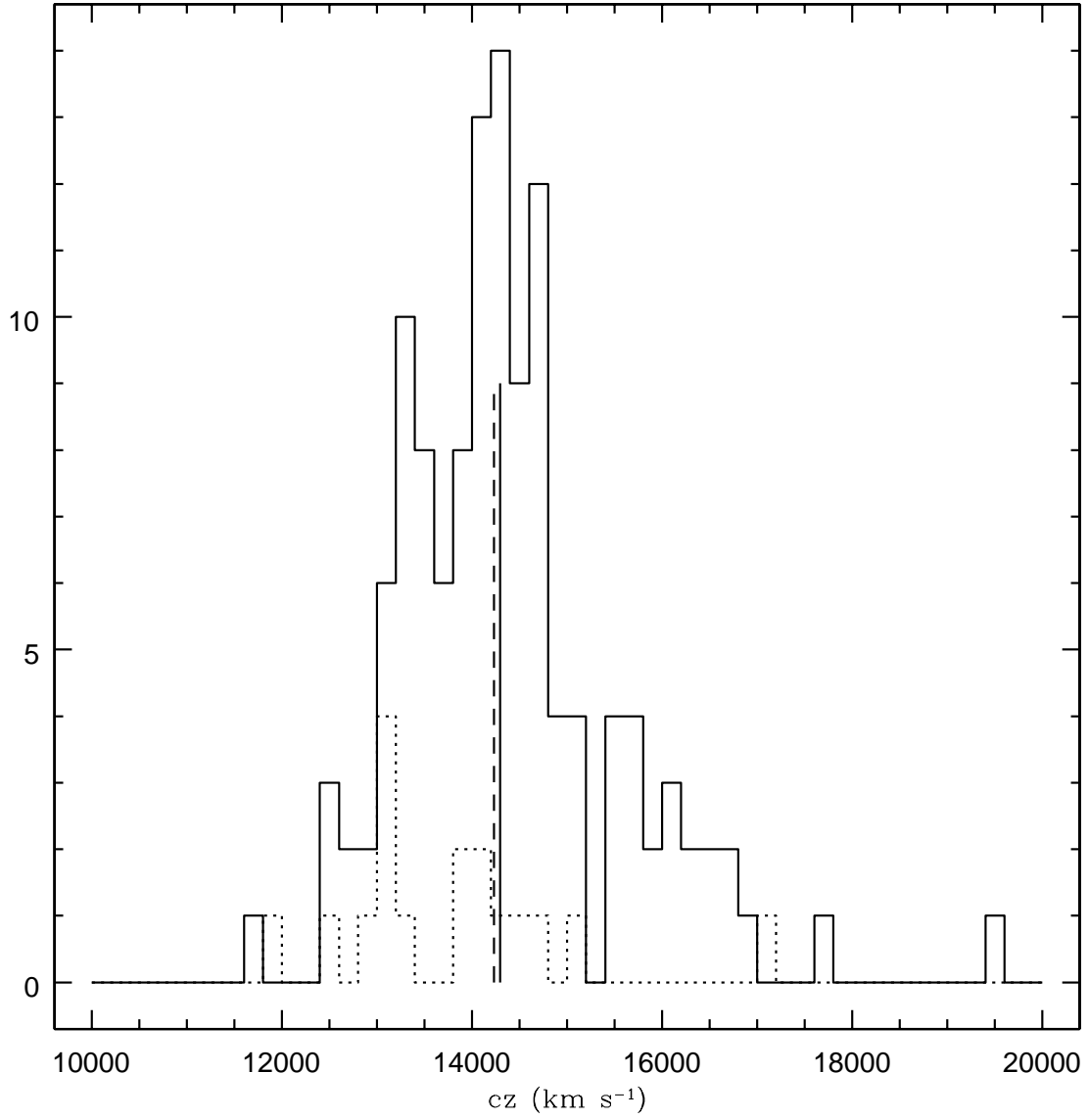


Fig. 4.— Velocity distribution of the cluster sample separated by spectral type. Solid histogram: 123 Abs galaxies. Dotted histogram: 18 Em galaxies. Solid and dashed vertical lines indicate the mean velocity of the cluster and the velocity of the cD, respectively.

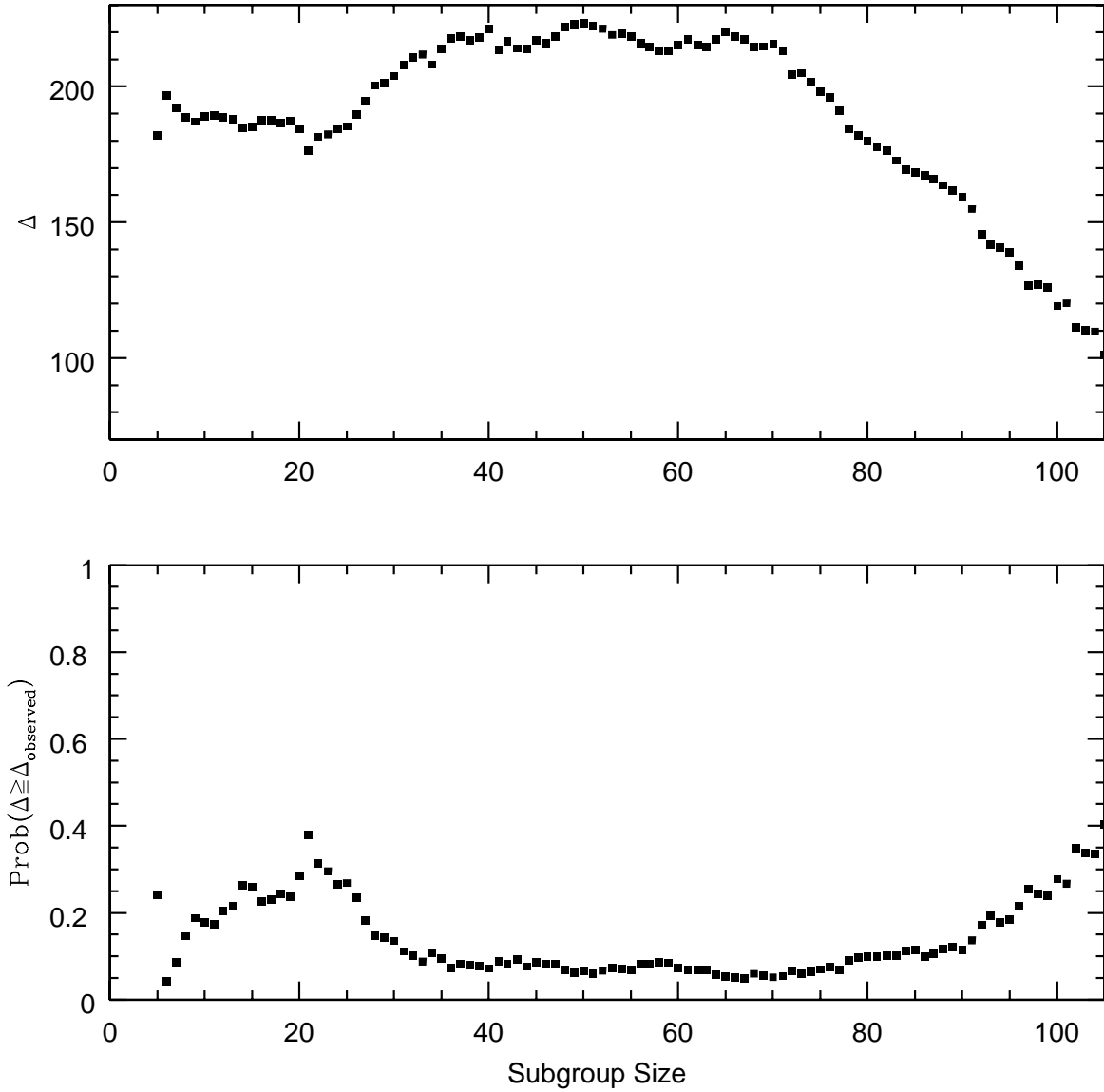


Fig. 5.— Top: Value of the Dressler-Shectman statistic  $\Delta$  for varying subgroup size  $n$ . Bottom: Probability that  $\Delta \geq \Delta_{\text{observed}}$ , based on 5000 Monte Carlo models for each value of  $n$ . With  $n = 11$  our analysis does not confirm the detection of substructure by Dressler & Shectman (1988b).

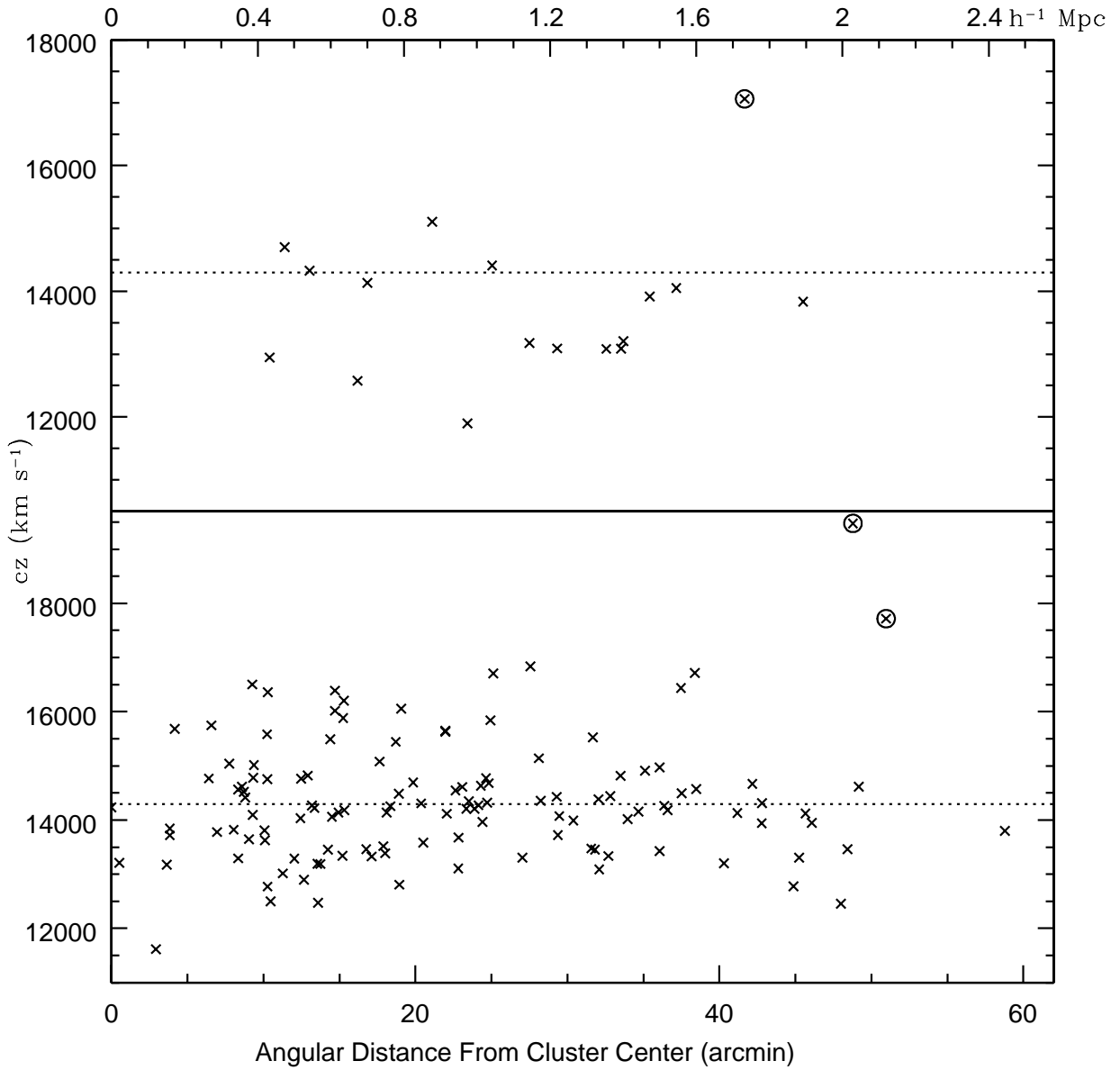


Fig. 6.— Radial velocity profile of Em (top) and Abs (bottom) galaxies. The horizontal dotted line shows the mean velocity of the cluster. There are three circled galaxies which may be outliers.

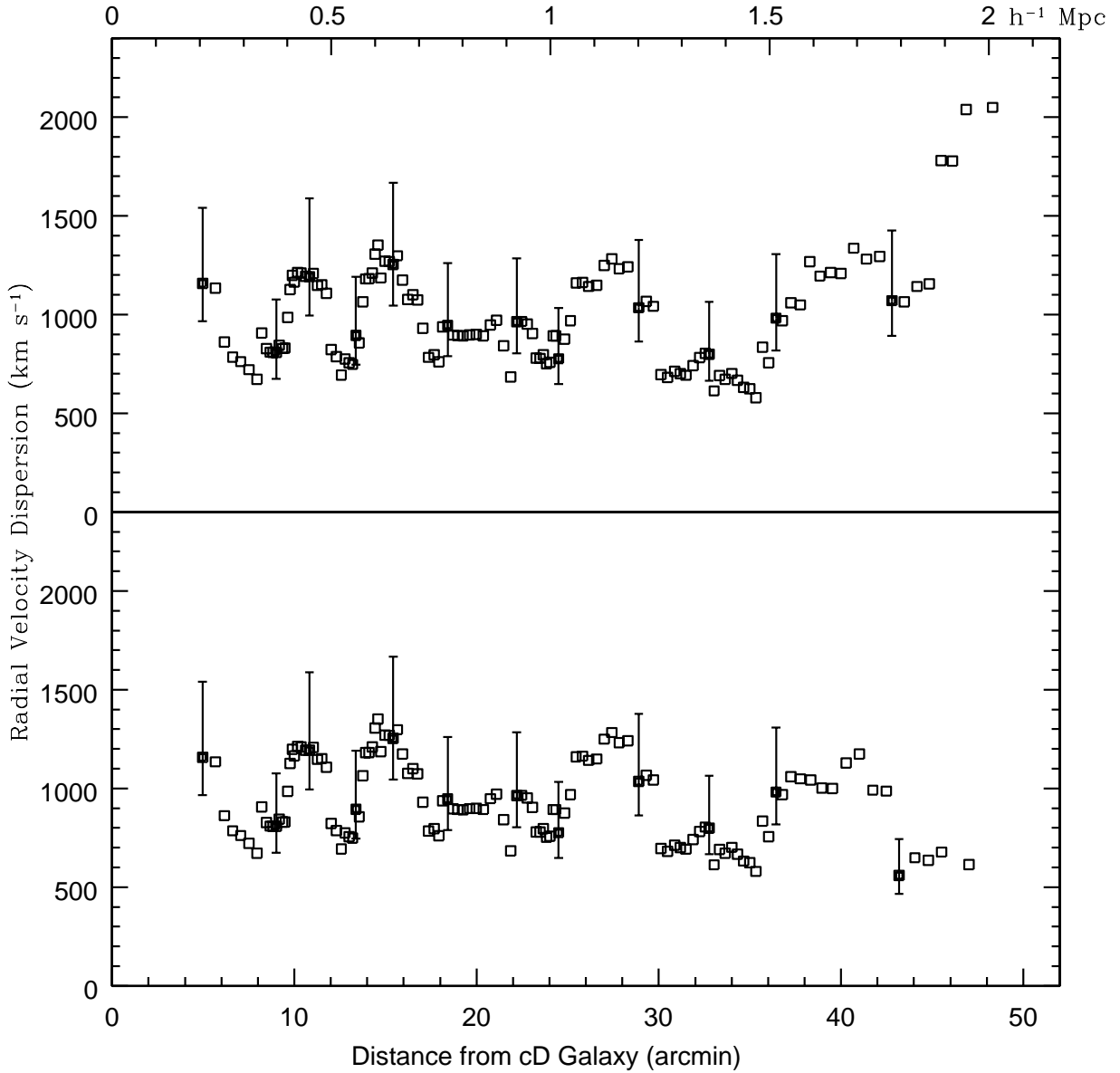


Fig. 7.— Velocity dispersion for groups of 11 galaxies moving outward from the cD. Error bars show 68% confidence levels for uncorrelated samples. Top: Includes all 141 galaxies with  $10,000 \text{ km s}^{-1} < cz < 20,000 \text{ km s}^{-1}$ . Bottom: Excludes the three high-velocity outliers circled in Figure 6.

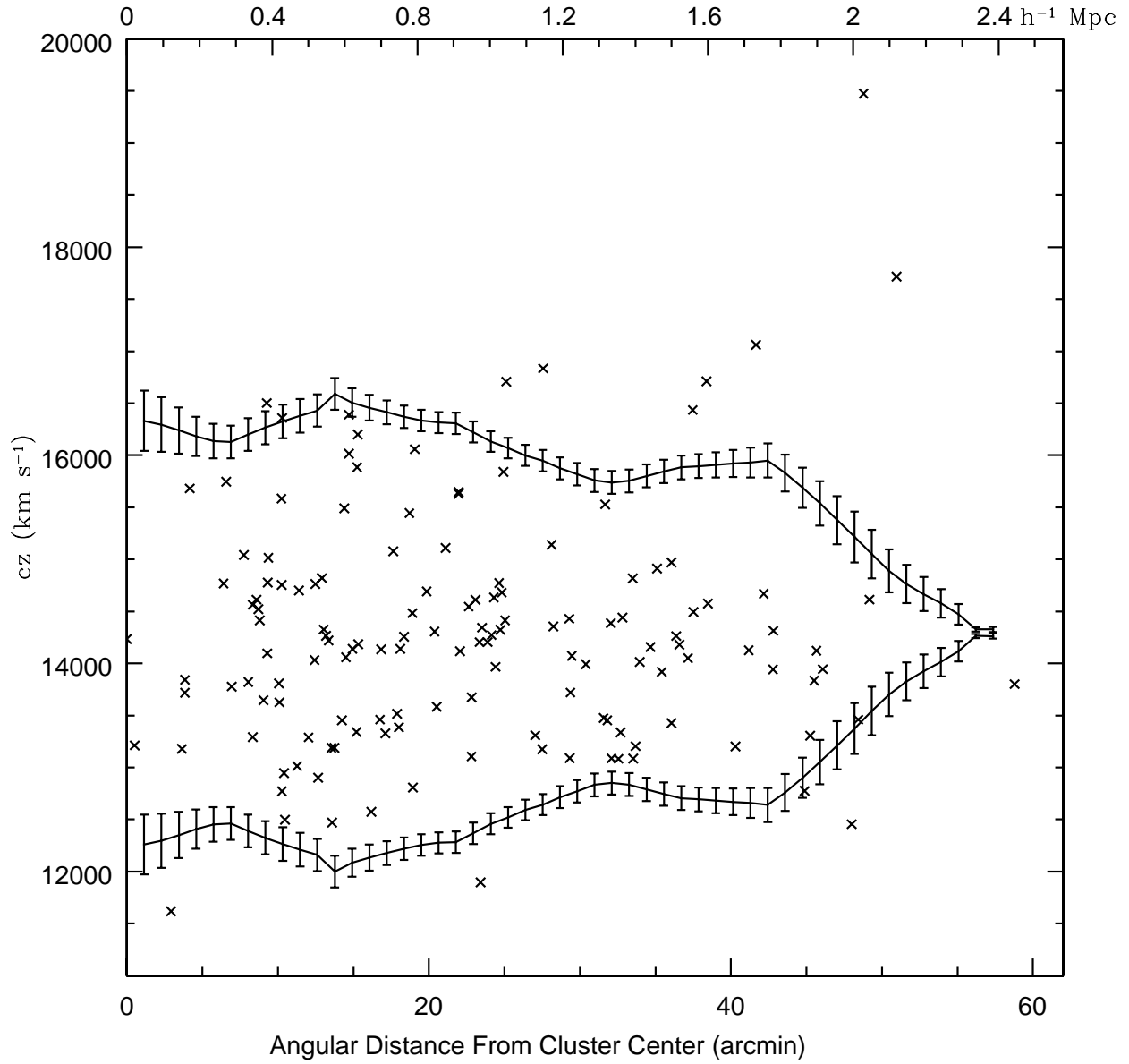


Fig. 8.— Caustics and cluster members in position-redshift space. The caustic curves  $A(R)$  are shown as solid lines with  $1\sigma$  error bars.



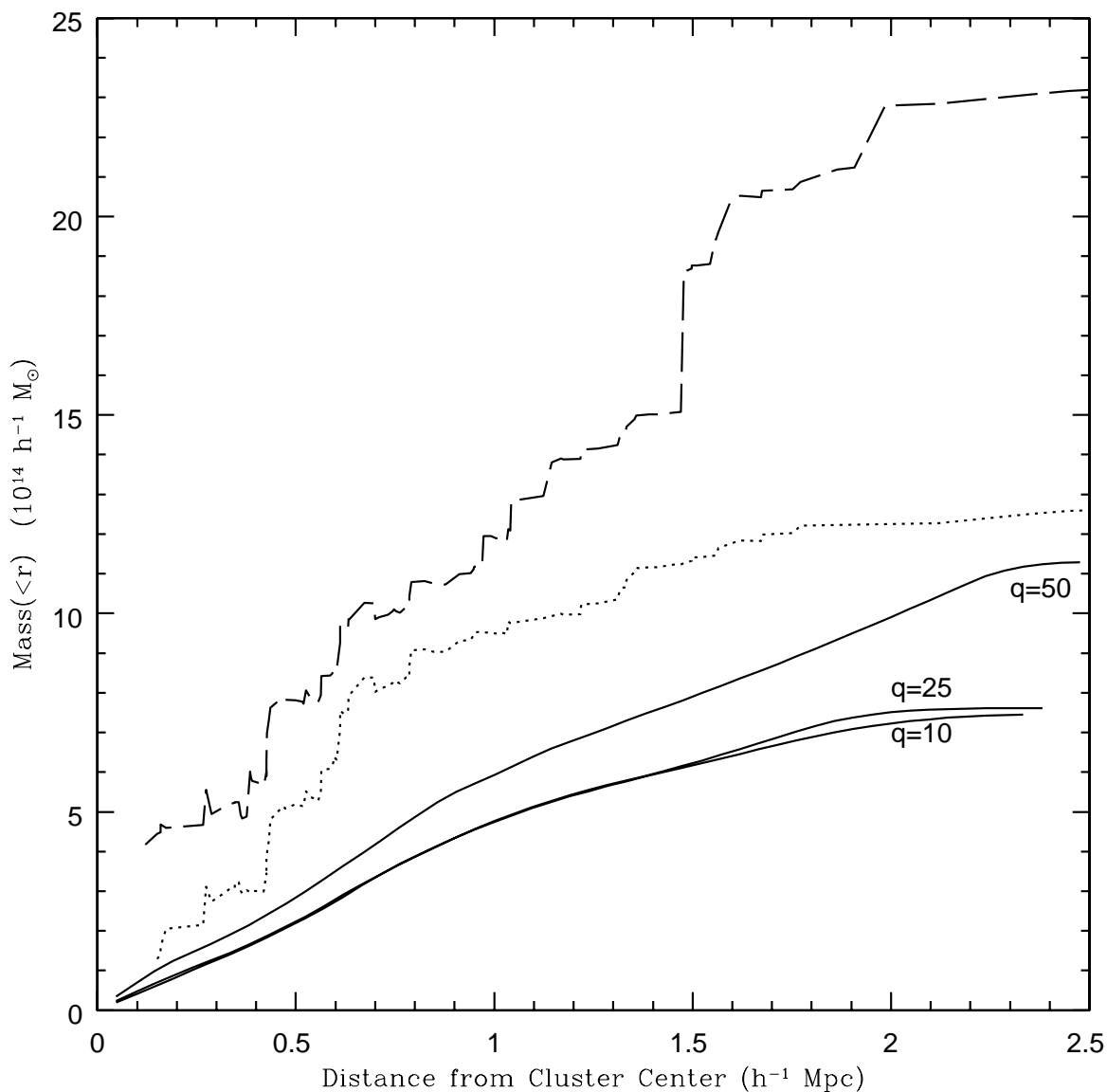


Fig. 9.— Virial and caustic masses illustrating the inherent uncertainties in each technique. Solid lines: caustic mass calculated with smoothing parameter  $q=10$ ,  $25$ , and  $50$ . Dashed line: virial mass including 141 galaxies with  $10,000 \text{ km s}^{-1} < cz < 20,000 \text{ km s}^{-1}$ . Dotted line: virial mass using only galaxies which lie within the  $q=25$  caustics.

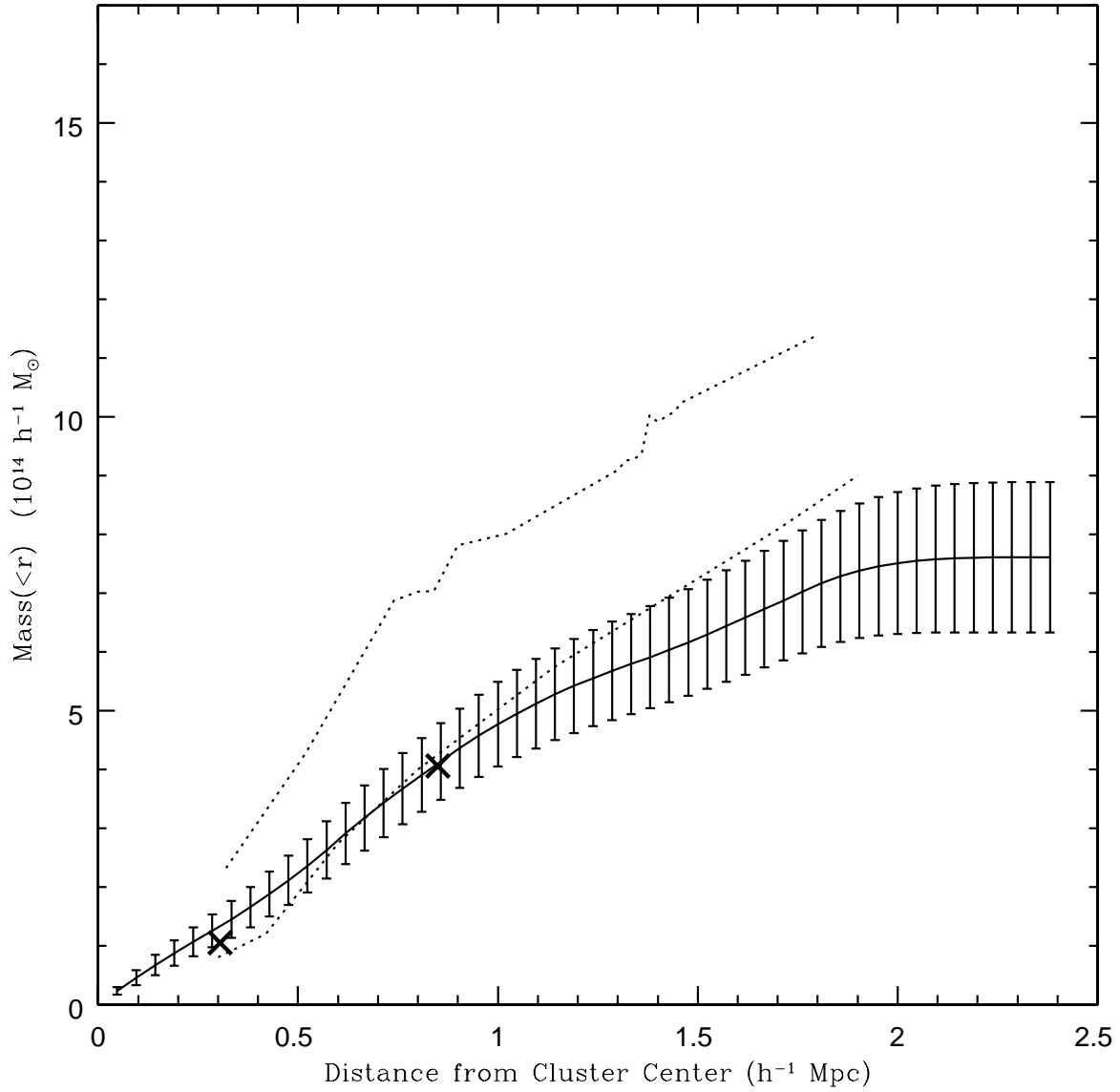


Fig. 10.— Radial mass profile of A1644. Solid line represents the caustic estimate; dotted lines show upper and lower envelopes of the virial estimate with surface term correction. Crosses show the X-ray determinations from Ettori, Fabian, & White (1997).

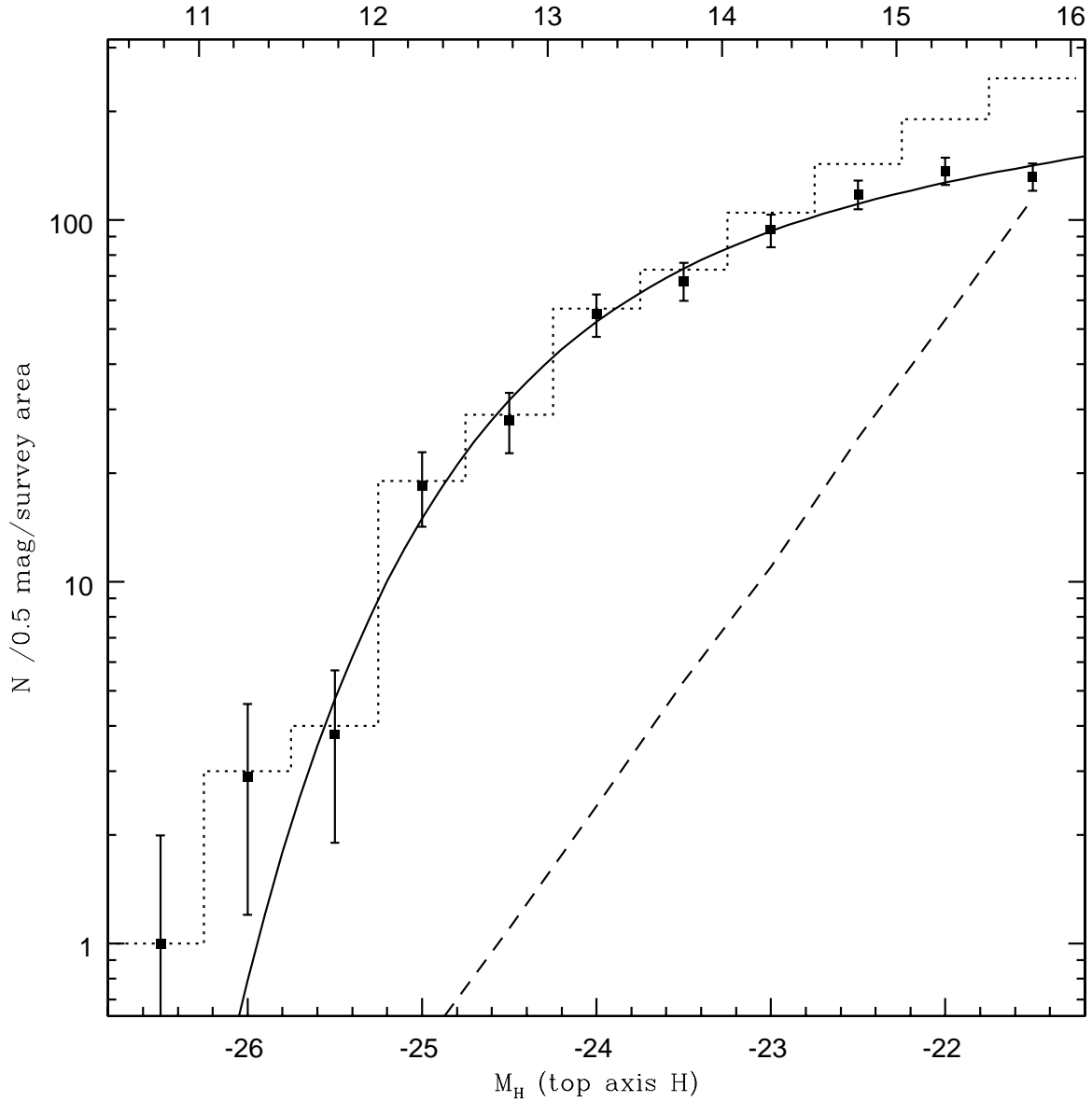


Fig. 11.— Differential  $H$ -band luminosity function. Dotted histogram: all objects classified as galaxies by the SExtractor CLASS\_STAR parameter. Dashed line: background counts modeled as a  $10^{0.67m}$  power law. Filled squares with error bars: number of cluster members in each bin after background subtraction. Solid curve: best-fit Schechter function.

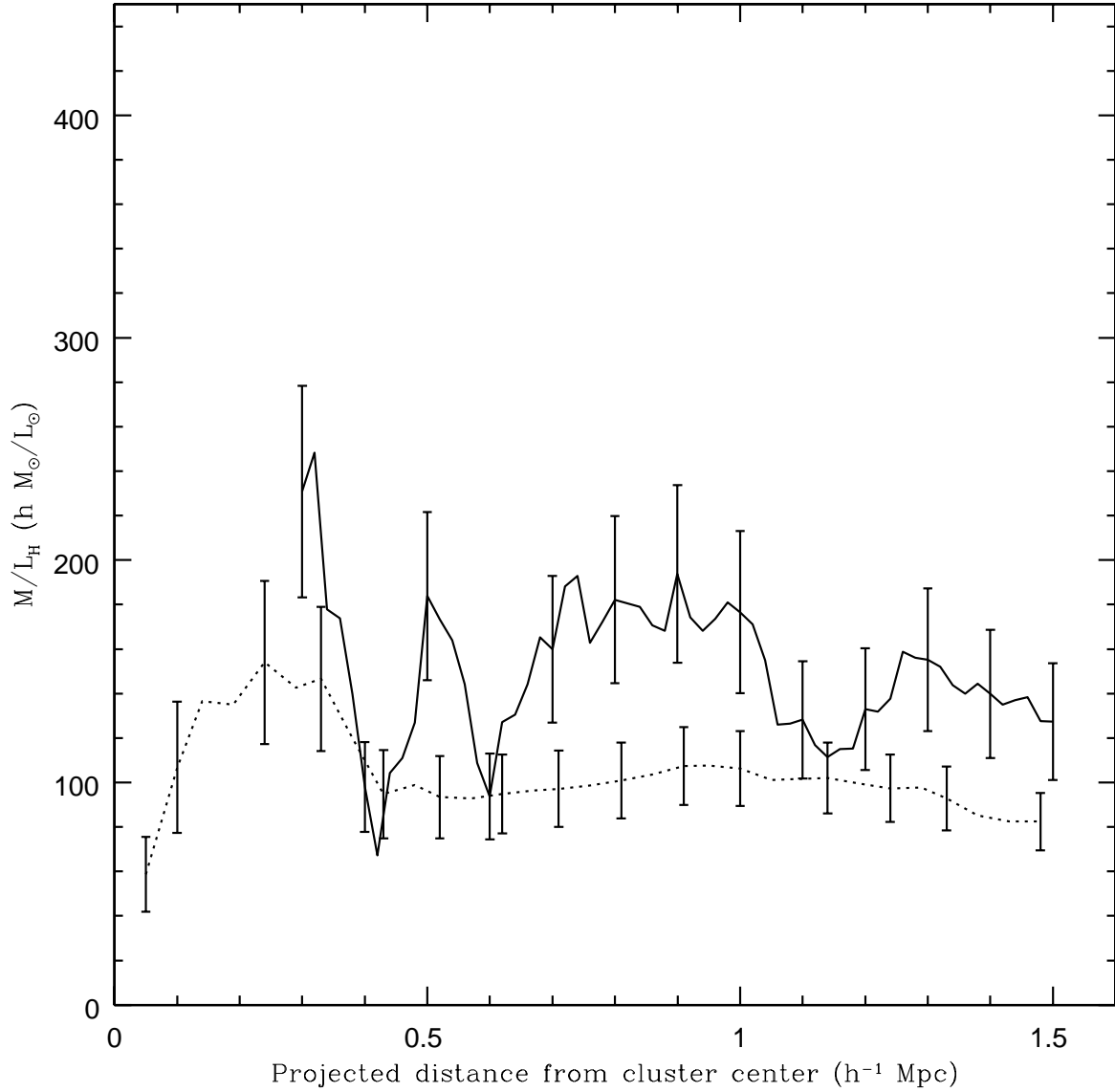


Fig. 12.— Mass-to-light ratio as a function of projected radius. Solid and dotted lines represent  $M/L_H$  computed with virial and caustic mass estimates, respectively. We show characteristic error bars at several locations along each curve.

Table 1. Properties of Photometric Sample

RA (J2000)	Dec. (J2000)	$m_H$	$cz$ km s <sup>-1</sup>
(1)	(2)	(3)	(4)
12 54 50.9	-17 01 28.6	14.46	...
12 54 51.4	-16 57 34.6	15.19	...
12 54 57.9	-17 00 59.0	15.15	...
12 55 06.2	-17 42 23.0	13.97	14971

Note. — The complete version of this table is in the electronic edition of the Journal. The printed edition contains only a sample.

Table 2. Properties of Spectroscopic Sample

RA (J2000) (1)	Dec. (J2000) (2)	$cz$ (km s <sup>-1</sup> ) (3)	$\sigma_{cz}$ (km s <sup>-1</sup> ) (4)	Type (5)	$m_H$ (6)	DS Number (7)
12 58 35.9	-18 04 11.8	12774	33	Abs	13.18	1
12 56 10.2	-17 59 44.7	16712	36	Abs	14.20	2
12 56 54.5	-17 56 51.2	13083	16	Em	12.16	6
12 52 20.9	-17 39 16.0	13306	34	Abs	...	9
12 57 20.7	-17 52 36.4	15140	33	Abs	13.86	12

Note. — The complete version of this table is in the electronic edition of the Journal. The printed edition contains only a sample.